

Towards an effective field theory approach to the neutrinoless double-beta decay

Mihai Horoi* and Andrei Neacsu†

Department of Physics, Central Michigan University, Mount Pleasant, Michigan 48859, USA

(Dated: October 12, 2018)

Weak interaction in nuclei represents a well-known venue for testing many of the fundamental symmetries of the Standard Model. In particular, neutrinoless double-beta decay offers the possibility to test Beyond Standard Model theories predicting that neutrinos are Majorana fermions and the lepton number conservation is violated. This paper focuses on an effective field theory approach to neutrinoless double-beta decay for extracting information regarding the properties of the Beyond Standard Model Lagrangian responsible for this process. We use shell model nuclear matrix elements and the latest experimental lower limits for the half-lives to extract the lepton number violating parameters of five nuclei of experimental interest, and lower limits for the energy scales of the new physics.

I. INTRODUCTION

The neutrinoless double-beta decay ($0\nu\beta\beta$) is considered the best approach to study the yet unknown properties of neutrinos related to their nature, whether they are Dirac or Majorana fermions, which the neutrino oscillation experiments cannot clarify. Should the neutrinoless double-beta transitions occur, then the lepton number conservation is violated by two units, and the black-box theorems [1–4] indicate that the light left-handed neutrinos are Majorana fermions. As such, through black-box theorems alone, it is not possible to disentangle the dominant mechanism contributing to this process. Most of the theoretical effort dedicated to this subject consists of calculations of leptonic phase-space factors and nuclear matrix elements that are computed via several nuclear structure methods and within specific models. One of the most popular models is the left-right symmetric model [5–9], which is currently investigated at the Large Hadron Collider (LHC) [10]. In two recent papers [11, 12] we have discussed ways to identify some of the possible contributions to the decay rate by studying the angular distribution and the energy distribution of the two outgoing electrons that could be measured. However, there are still many other possible contributions to this process that one cannot yet dismiss. For these reasons, a more general beyond standard model (BSM) effective field theory would be preferable, as it would not be limited to relying on specific models, but rather considering the most general BSM effective field theoretical approach that describes this process. An important outcome of such a theory is the evaluation of the energy scales up to which the effective field operators are not broken, together with limits for the effective low-energy couplings.

The analysis of the $0\nu\beta\beta$ decay process is generally done at three levels. At the lowest level the weak interaction of the quarks and leptons is considered and the BSM physics is treated within a low-energy effective

field theory approach. At the next level the hadronization process to nucleons and exchanging pion is considered. The nucleons are treated in the impulse approximation leading to free space $0\nu\beta\beta$ transition operators. At the third level the nucleon dynamics inside the nuclei is treated using nonperturbative nuclear wave functions, which are further used to obtain nuclear matrix elements (NME) needed to calculate the $0\nu\beta\beta$ observables, such as half-lives and two-electron angular and energy distributions [11]. A modern approach that could accomplish this plan would be based on the chiral effective field theory of pions and nucleons [13, 14]. This approach introduces a number of couplings, which in principle can be calculated from the underlying theory of strong interaction using lattice QCD techniques [13], or may be extracted within some approximation from the known experimental data [14]. These couplings may come with new phases and they may include effective contributions from the exchange of heavier mesons. The lattice QCD approach is underway, but it proved to be very difficult for extracting even basic weak nucleon couplings, such as g_A [15].

In this paper we start from the formalism of Ref. [16–19] that provides a general effective field theory (EFT) approach to the neutrinoless double-beta decay. However, at the hadron level three new diagrams are added for the first time to the effective field theory analysis of the $0\nu\beta\beta$, which were only considered in the literature in the context of specific mechanisms. Under the assumption that a single coupling in the BSM Lagrangian dominates the $0\nu\beta\beta$ amplitude, we extract new limits for the effective Majorana mass and for 11 additional low-energy EFT couplings using data from five nuclei of current experimental interest. Some of these couplings correspond to parameters found in left-right symmetric models, and we present and compare them. To be able to get the limits of these effective couplings and parameters from the experimental half-life limits, 23 nuclear matrix elements (NME) and 9 phase-space factors (PSF) are needed. Finally, we use the limits for the EFT couplings and the formalism of the effective field theory to obtain limits for the energy scale of the new physics that could be responsible for the neutrinoless double beta decay process.

To accomplish this goal we need reliable NME. The

* mihai.horoi@cmich.edu

† neacs1a@cmich.edu

most commonly used nuclear structure methods for the NME calculation are proton-neutron Quasi Random Phase Approximation (pnQRPA) [16–24], Interacting Shell Model (ISM) [25–43], Interacting Boson Model (IBM-2) [44–47], Projected Hartree Fock Bogoliubov (PHFB) [48], Energy Density Functional (EDF) [49], and the Relativistic Energy Density Functional (REDF) [50] method. The NME calculated with different methods and by different groups sometimes show large differences, and this has been debated in the literature [51, 52]. Although there seem to exist many NME results to choose from, most of the references listed only provide calculations for the light left-handed Majorana neutrino exchange. Ref. [41] provides tables and plots that compare the latest results for the light left-handed neutrino exchange and for the heavy right-handed neutrino exchange.

The NME used in Ref. [16–19] come from older QRPA calculations, which do not include many of the improvements proposed in recent years [53, 54]. We calculate the NME using shell model techniques, which are consistent with previous calculations [27, 32–42]. The reason for choosing shell model NME is our belief that these are better suited and more reliable for $0\nu\beta\beta$ calculations, as they take into account all the correlations around the Fermi surface, respect all symmetries, and take into account consistently the effects of the missing single particle space via many-body perturbation theory (the effects were shown to be small, about 20%, for ^{82}Se [55]). Furthermore, we have tested the shell model methods and the effective Hamiltonians used by comparing calculations of spectroscopic observables to the experimental data, as presented in Ref. [32, 41, 56]. We do not consider any quenching for the bare $0\nu\beta\beta$ operator in these calculations. Such a choice is different from that for the simple Gamow-Teller operator used in the single beta and $2\nu\beta\beta$ decays where a quenching factor of about 0.7 is necessary [57]. For the PSF we use an effective theory based on the formalism of Ref. [58], but fine-tuned as to take into account the effects of a Coulomb field distorting finite-size proton distribution in the final nucleus. To our knowledge, some of the NME presented in this paper are calculated for the first time using shell model techniques.

This paper is organized as follows: Section II analyzes the contributions of several BSM mechanisms to the neutrinoless double-beta decay. Section III presents the framework of the effective field theory for the neutrinoless double-beta decay. Section IV shows the experimental limits on the BSM lepton number violating (LNV) couplings that we calculate, and is divided into three subsections. Subsection IV A is dedicated to the revisit of the most common approach to $0\nu\beta\beta$ that considers only the light left-handed Majorana neutrino exchange, presenting shell model nuclear matrix elements and upper limits for the Majorana mass. Subsection IV B details the study of the long-range contributions to the $0\nu\beta\beta$ decay Lagrangian. Subsection IV C presents the analysis of the short-range contribution LNV parameters. Discuss-

sions are presented in Section V, Section VI is dedicated to conclusions and, last, Section VII is an Appendix containing all the relevant formulae for calculating the NME.

II. BSM MECHANISMS CONTRIBUTING TO NEUTRINOLESS DOUBLE-BETA DECAY

The main mechanism considered to be responsible for the neutrinoless double beta decay is the mass mechanism that assumes that the neutrinos are Majorana fermions, and relies on the assumption that the light left-handed neutrinos have mass. However, the possibility that right-handed currents could contribute to the neutrinoless double-beta decay ($0\nu\beta\beta$) has been already considered for some time [58, 65]. Recently, $0\nu\beta\beta$ studies [9, 66] have adopted the left-right symmetric model [7, 67] for the inclusion of right-handed currents. In addition, the R -parity violating (\mathcal{K}_p) supersymmetric (SUSY) model can also contribute to the neutrinoless double beta decay process [68–70]. In the framework of the left-right symmetric model and R -parity violating SUSY model, the $0\nu\beta\beta$ half-life can be written as a sum of products of PSF, BSM LNV parameters, and their corresponding NME [11]:

$$\left[T_{1/2}^{0\nu} \right]^{-1} = G_{01} g_A^4 \left| \eta_{0\nu} M_{0\nu} + (\eta_{N_R}^L + \eta_{N_R}^R) M_{0N} \right. \\ \left. + \eta_{\tilde{q}} M_{\tilde{q}} + \eta_{\lambda'} M_{\lambda'} + \eta_\lambda X_\lambda + \eta_\eta X_\eta \right|^2. \quad (1)$$

Here, G_{01} is a phase-space factor that can be calculated with good precision for most cases [59, 71–73], g_A is the axial vector coupling constant, $\eta_{0\nu} = \frac{\langle m_{\beta\beta} \rangle}{m_e}$, with $\langle m_{\beta\beta} \rangle$ representing the effective Majorana neutrino mass, and m_e the electron mass. $\eta_{N_R}^L$, $\eta_{N_R}^R$ are the heavy neutrino parameters with left-handed and right-handed currents, respectively [9, 27], $\eta_{\tilde{q}}$, $\eta_{\lambda'}$ are \mathcal{K}_p SUSY LNV parameters [74], η_λ , and η_η are parameters for the so-called “ λ –” and “ η –mechanism”, respectively [9]. $M_{0\nu}$, M_{0N} , are the light and the heavy neutrino exchange NME, $M_{\tilde{q}}$, $M_{\lambda'}$ are the \mathcal{K}_p SUSY NME, and X_λ and X_η denote combinations of NME and other PSF ($G_{02} - G_{09}$) corresponding to the the λ –mechanism involving right-handed leptonic and right-handed hadronic currents, and the η –mechanism with right-handed leptonic and left-handed hadronic currents, respectively [11]. The heavy neutrino exchange contribution to the amplitude in Eq. 1 proportional with M_N assumes that the heavy neutrino masses are larger than ≈ 1 GeV and the information about their mass is included into the couplings[11].

In Table I we present the $Q_{\beta\beta}^{0\nu}$ values, the most recent experimental half-life limits from the indicated references, and the nine PSF for $0\nu\beta\beta$ transitions to ground states of the daughter nucleus for five isotopes currently under investigation. The PSF were calculated using a new effective method described in great detail in Ref. [73]. G_{01} values were calculated with a screening factor (s_f) of 94.5, while for $G_{02} - G_{09}$ we used $s_f = 92.0$ that was

TABLE I. The $Q_{\beta\beta}^{0\nu}$ values in MeV, the experimental $T_{1/2}^{0\nu}$ limits in years, and the calculated PSF ($G_{01} - G_{09}$) in years $^{-1}$ for all five isotopes currently under investigation.

	^{48}Ca	^{76}Ge	^{82}Se	^{130}Te	^{136}Xe
$Q_{\beta\beta}^{0\nu}$ [59]	4.272	2.039	2.995	2.813	2.287
$T_{1/2}^{0\nu} >$	$2.0 \cdot 10^{22}$ [60]	$5.3 \cdot 10^{25}$ [61]	$2.5 \cdot 10^{23}$ [62]	$4.0 \cdot 10^{24}$ [63]	$1.07 \cdot 10^{26}$ [64]
$G_{01} \cdot 10^{14}$	2.45	0.22	1.00	1.41	1.45
$G_{02} \cdot 10^{14}$	15.4	0.35	3.21	3.24	3.15
$G_{03} \cdot 10^{15}$	18.2	1.20	6.50	8.46	8.55
$G_{04} \cdot 10^{15}$	5.04	0.42	1.92	2.53	2.58
$G_{05} \cdot 10^{13}$	3.28	0.60	2.16	4.12	4.36
$G_{06} \cdot 10^{12}$	3.87	0.50	1.65	2.16	2.21
$G_{07} \cdot 10^{10}$	2.85	0.28	1.20	1.75	1.80
$G_{08} \cdot 10^{11}$	1.31	0.17	0.82	1.72	1.83
$G_{09} \cdot 10^{10}$	15.5	1.12	4.42	4.47	4.44

shown to provide results very close to those of Ref. [75]. We note that the ^{82}Se experimental half-life used here and throughout this analysis is preliminary [62]. However, we believe that this limit is valid and that it may get improved.

In Ref. [11] we show how one could disentangle contributions from different mechanisms using two-electron angular and energy distributions, as well as half-life data from several isotopes. Here, we consider the case where one mechanism dominates, more explicitly, one single term in the decay amplitude of Eq. (1). Table II shows the shell model values of the NME that enter Eq. (1). The light and heavy neutrino-exchange NME, $M_{0\nu}$ and M_{0N} , are taken from Ref. [40] that describes their formalism and calculation. $M_{\tilde{q}}$ and $M_{\lambda'}$ are calculated using the description in Eq. (150) and Eq. (155), respectively, of Ref. [74]. X_{λ} and X_{η} are adapted from C_4 and C_5 of Eq. (3.5.15d) and Eq. (3.5.15e), respectively, in Ref. [58] multiplied by M_{GT}/G_{01} to fit the factorization of Eq. (1). All NME used in this paper were calculated using the interacting shell model (ISM) approach [27, 34–37, 40, 43] (see Ref. [40] for a review), and include short-range-correlation effects based on the CD-Bonn parametrization [32], finite-size effects [74] and, when appropriate, optimal closure energies [56] (see Appendix for more details).

The upper limits for corresponding LNV parameters extracted from lower limits of the half-lives under the assumption that only one term in the amplitude dominates, are also presented in Table II. There are a few other QRPA [58, 74–77] and ISM [25–28] results in the literature that were obtained within the framework of the LRSM and SUSY. However, some of the extracted LNV parameters rely on some older half-life limits.

TABLE II. The NME that appear in Eq. (1) for the five nuclei of current experimental interest, and the corresponding LNV parameters extracted under the assumption that only one dominates.

	^{48}Ca	^{76}Ge	^{82}Se	^{130}Te	^{136}Xe
$M_{0\nu}$	1.03	3.64	3.41	1.93	1.75
M_{0N}	75.5	202	187	136	122
$M_{\tilde{q}}$	107	339	320	185	169
$M_{\lambda'}$	370	619	570	415	366
X_{λ}	2.11	4.12	5.68	2.81	2.48
X_{η}	246	794	725	517	467
$10^6 \cdot \eta_{0\nu} $	27.1	0.49	3.64	1.36	0.28
$10^9 \cdot \eta_{0N} $	370.6	8.83	66.3	19.2	4.01
$10^9 \cdot \eta_{\tilde{q}} $	260	5.26	38.8	14.1	2.91
$10^9 \cdot \eta_{\lambda'} $	75.7	2.88	21.8	6.29	1.34
$10^7 \cdot \eta_{\lambda} $	133	4.32	21.87	9.29	1.98
$10^9 \cdot \eta_{\eta} $	114	2.25	17.1	5.05	1.05

III. EFFECTIVE FIELD THEORY APPROACH TO NEUTRINOLESS DOUBLE-BETA DECAY

A more general approach is based on the effective field theory extension of the Standard Model. The analysis based on the BSM contributions to the effective field theory is more desirable, because it does not rely on specific models, and their parameters could be extracted/constrained by the existing $0\nu\beta\beta$ data, and by data from LHC and other experiments. In fact, the models considered in section II always lead to a subset of terms in the low-energy (~ 200 MeV) effective field theory Lagrangian. Here we consider all the terms in the Lagrangian allowed by the symmetries. Some of the couplings will correspond to the model couplings in Eq. (1), but they might have a wider meaning. Others are new, not corresponding to specific models.

At the quark-level, we present in Figure 1 the generic $0\nu\beta\beta$ Feynman diagrams contributing to the $0\nu\beta\beta$ pro-

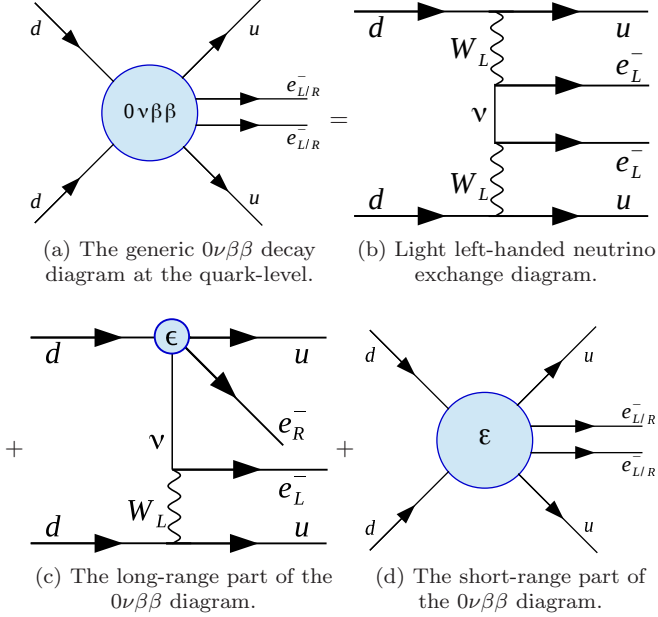


FIG. 1. The $0\nu\beta\beta$ decay process diagrams: (1a) presents the generic description of the process, (1b) shows the most studied case in the literature, that of the light left-handed neutrino exchange, (1c) is the long-range component of the $0\nu\beta\beta$ decay diagram, while (1d) displays the short-range part.

cess. We consider contributions coming from the light left-handed Majorana neutrino (Fig. 1b), a long-range part coming from the low-energy four-fermion charged-current interaction (Fig. 1c), and a short-range part (Fig. 1d).

We treat the long-range component of the $0\nu\beta\beta$ diagram as two point-like vertices at the Fermi scale, which exchange a light neutrino. In this case, the dimension 6 Lagrangian can be expressed in terms of effective couplings [19]:

$$\mathcal{L}_6 = \frac{G_F}{\sqrt{2}} \left[j_{V-A}^\mu J_{V-A,\mu}^\dagger + \sum_{\alpha,\beta}^* \epsilon_\alpha^\beta j_\beta J_\alpha^\dagger \right], \quad (2)$$

where $J_\alpha^\dagger = \bar{u} \mathcal{O}_\alpha d$ and $j_\beta = \bar{e} \mathcal{O}_\beta \nu$ are hadronic and leptonic Lorentz currents, respectively. The definitions of the $\mathcal{O}_{\alpha,\beta}$ operators are given in Eq. (3) of Ref. [19]. The LNV parameters are $\epsilon_\alpha^\beta = \{\epsilon_{V-A}^{V+A}, \epsilon_{V+A}^{V+A}, \epsilon_{S\pm P}^{S+P}, \epsilon_{TL}^{TR}, \epsilon_{TR}^{TR}\}$. The “*” symbol indicates that the term with $\alpha = \beta = (V - A)$ is explicitly taken out of the sum. However, the first term in Eq. (2) still entails BSM physics through the dimension-5 operator responsible for the Majorana neutrino mass (see also section V). Here $G_F = 1.1663787 \times 10^{-5} \text{ GeV}^{-2}$ denotes the Fermi coupling constant.

As already mentioned, some of these couplings play the same role as some of the model couplings listed in Eq. (1), but they have more general meaning here. For example, ϵ_{V-A}^{V+A} play the same role as η_η and ϵ_{V+A}^{V+A} play

the same role as η_λ in the effective Lagrangian associated to models.

In the short-range part of the diagram presented in Fig. 1d we consider the interaction to be point-like. Expressing the general Lorentz-invariant Lagrangian in terms of effective couplings [18], we get:

$$\mathcal{L}_9 = \frac{G_F^2}{2m_p} \left[\varepsilon_1 J J j + \varepsilon_2 J^{\mu\nu} J_{\mu\nu} j + \varepsilon_3 J^\mu J_{\mu} j \right. \\ \left. + \varepsilon_4 J^\mu J_{\mu\nu} j^\nu + \varepsilon_5 J^\mu J j_\mu \right], \quad (3)$$

with the hadronic currents of defined chirality $J = \bar{u}(1 \pm \gamma_5)d$, $J^\mu = \bar{u}\gamma^\mu(1 \pm \gamma_5)d$, $J^{\mu\nu} = \bar{u}\frac{i}{2}[\gamma^\mu, \gamma^\nu](1 \pm \gamma_5)d$, leptonic currents $j = \bar{e}(1 \pm \gamma_5)e^C$, $j^\mu = \bar{e}\gamma^\mu(1 \pm \gamma_5)e^C$, and $\varepsilon_\alpha^\beta = \varepsilon_{xyz}^{LLz(RRz)} = \{\varepsilon_1, \varepsilon_2, \varepsilon_3^{LLz(RRz)}, \varepsilon_3^{LRz(RLz)}, \varepsilon_4, \varepsilon_6\}$. These parameters have dependence on the chirality of the hadronic and the leptonic currents involved, with $xyz = L/R, L/R, L/R$. In the case of ε_3 , one can distinguish between different chiralities, thus we express them separately as $\varepsilon_3^{LLz(RRz)}$ and $\varepsilon_3^{LRz(RLz)}$.

The contribution of the diagrams 1b and 1c to the $0\nu\beta\beta$ decay amplitude is proportional to the time-ordered product of two effective \mathcal{L}_6 Lagrangians [19],

$$T(\mathcal{L}_6^{(1)} \mathcal{L}_6^{(2)}) = \frac{G_F^2}{2} T \left[j_{V-A} J_{V-A}^\dagger j_{V-A} J_{V-A}^\dagger \right. \\ \left. + \epsilon_\alpha^\beta \epsilon_\gamma^\delta j_\beta J_\alpha^\dagger j_{V-A}^\dagger + \epsilon_\alpha^\beta \epsilon_\gamma^\delta j_\beta J_\alpha^\dagger j_\delta J_\gamma^\dagger \right], \quad (4)$$

while the contribution of the diagram 1d is proportional to \mathcal{L}_9 .

However, when calculating the $0\nu\beta\beta$ half-life it is necessary to identify the contributions corresponding to different hadronization prescriptions. Figure 2 shows the nucleon-level diagrams in a similar way to Figure 1. The first 3 contributions, Figs. 2b, 2c, and 2d are similar to the corresponding amplitudes at the quark level (see Fig. 1). In addition to these contributions that were also considered in Ref. [19], here we also include the long range diagrams that involve pion(s) exchange, Figs. 2e, 2f, and 2g. These diagrams were considered before as contributing to the $0\nu\beta\beta$ decay rate, but in the context of \mathcal{K}_p SUSY mechanism. For example, the diagram 2e was considered to describe the contribution of the squark-exchange mechanism [70], and the diagrams 2f and 2g were considered to describe the contribution of the gluino exchange mechanism [78]. One should also mention that the diagram 2g was also considered in Refs. [79, 80], but its contribution to the $0\nu\beta\beta$ half-life was estimated differently, and cannot be directly compared to the other contributions analyzed here.

After hadronization (see Fig. 2), the extra terms in the Lagrangian require the knowledge of 23 individual NME [17–19, 68, 74, 81]. We can write the half-life in a factorized compact form

$$\left[T_{1/2}^{0\nu} \right]^{-1} = g_A^4 \left[\sum_i |\mathcal{E}_i|^2 \mathcal{M}_i^2 + \text{Re} \left[\sum_{i \neq j} \mathcal{E}_i \mathcal{E}_j \mathcal{M}_{ij} \right] \right]. \quad (5)$$

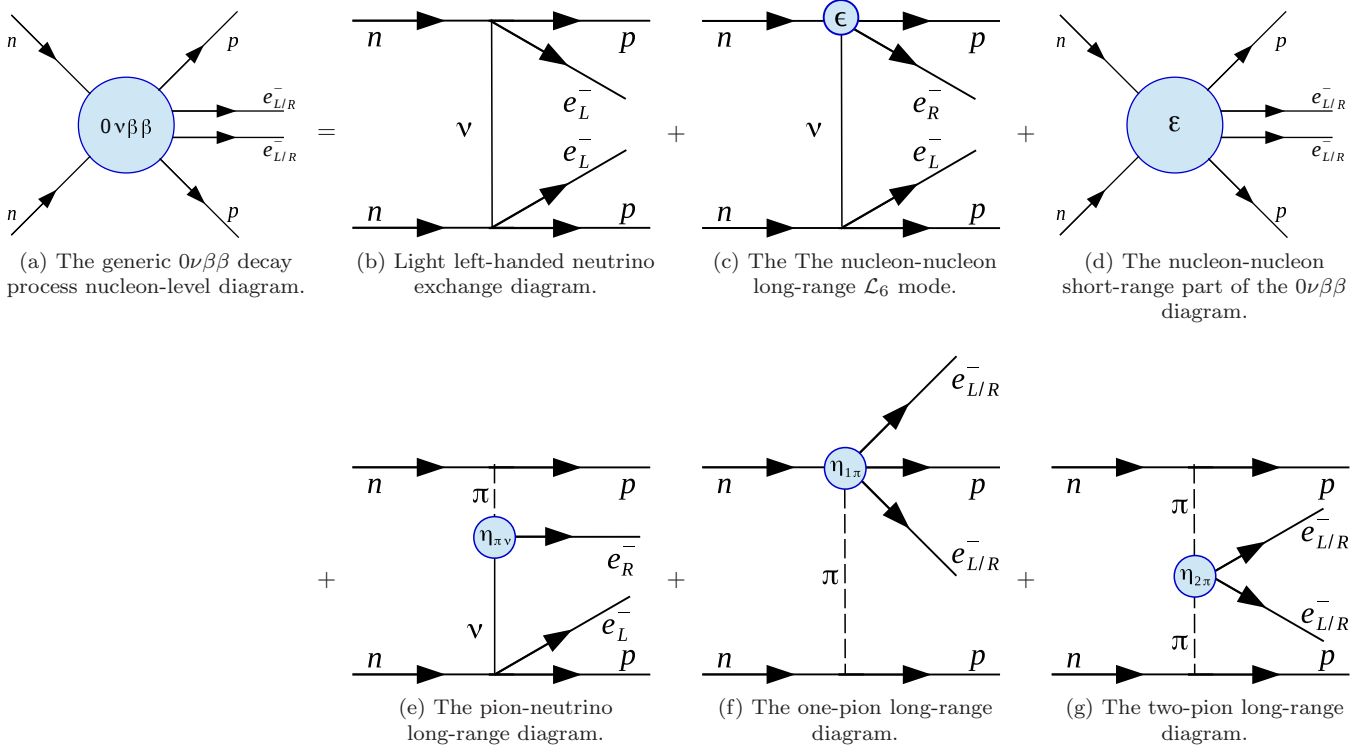


FIG. 2. Similar to Fig.1, we present the nucleon-level diagrams of $0\nu\beta\beta$ decay process : (2a) presents the generic description of the process, (2b) shows the light left-handed neutrino exchange, (2c) is the long-range component, Subfigure 2d shows the short-range contribution. On the second line, (2e) is the pion-neutrino component, (2f) is the one-pion long-range contribution of the \mathcal{R}_p SUSY induced $0\nu\beta\beta$ diagram, and (2g) presents the two-pion long-range contribution of the \mathcal{R}_p SUSY induced $0\nu\beta\beta$. The effective couplings $\eta_{1\pi}$ and $\eta_{2\pi}$ are related to Eq. (16) as $\eta_{1\pi} = c_{1\pi}\eta_{\pi N}$ and $\eta_{2\pi} = c_{2\pi}\eta_{\pi N}$.

Here, the \mathcal{E}_i contain the neutrino physics parameters, with $\mathcal{E}_1 = \eta_{0\nu}$ representing the exchange of light left-handed neutrinos corresponding to Fig. 2b, $\mathcal{E}_{2-7} = \{\epsilon_{V-A}^{V+A}, \epsilon_{V+A}^{V+A}, \epsilon_{S\pm P}^{S+P}, \epsilon_{TL}^{TR}, \epsilon_{TR}^{TR}, \eta_{\pi\nu}\}$ are the long-range LNV parameters appearing in Figs. 2c and 2e, and $\mathcal{E}_{8-15} = \{\varepsilon_1, \varepsilon_2, \varepsilon_3^{LLz(RRz)}, \varepsilon_3^{LRz(RLz)}, \varepsilon_4, \varepsilon_5, \eta_{1\pi}, \eta_{2\pi}\}$ denote the short-range LNV parameters at the quark level involved in the diagrams of Fig. 2d, 2f, 2g. The rational for including the $\eta_{\pi\nu}$ in the same class with the LNV entering the quark-level long range diagrams is that Ref. [70] indicates that $\eta_{\pi\nu}$ is proportional to ϵ_{TR}^{TR} (see Section IV B below). In the same vein, Ref. [78] indicates that ε_1 and ε_2 are proportional to a combination of $\eta_{1\pi}$ and $\eta_{2\pi}$ (see Section IV C below). Therefore the $\eta_{1\pi}$ and $\eta_{2\pi}$ were included in the list LNV couplings associated with quark-level short-range diagrams. Contributions of pion-exchange diagrams similar to those of Figs. 2f and 2g are also included in the so called "higher order term in nucleon currents" [74]. However, they are constrained by PCAC, and are only included in light-neutrino exchange contribution of diagram 2a. This contribution changes the associated NME by only 20%. Therefore, we conclude that this does not represent a serious double counting issue.

Following Refs. [17–19, 74], we write \mathcal{M}_i^2 as combina-

tions of NME described in Eqs. (8, 10, 12, 14, and 16) (see also Eq.(19) in the Appendix for the individual NME) and integrated PSF [73] denoted with $G_{01} - G_{09}$. Our values of the PSF are presented in Table I. In some cases the interference terms $\mathcal{E}_i\mathcal{E}_j\mathcal{M}_{ij}$ are small [82] and can be neglected, but not all of them. In Ref. [11] we analyzed a subset of terms contributing to the half-life formula, Eq. (1) originating from the left-right symmetric model. In that restrictive case we showed that one can disentangle different contributions to the $0\nu\beta\beta$ decay process using two-electron angular and energy distributions as well as half-lives of two selected isotopes. Obviously, this number of observables is not enough to extract all coupling appearing in the effective field theory Lagrangian. However, they can be used to constrain these couplings, thus adding to the information extracted from the Large Hadron Collider and other related experiments. Here we attempt to extract these couplings assuming that only one of them can have a dominant contribution to the half-life, Eq. (5). We call this approach "on-axis". Considering the "on-axis" approach to extracting limits of the LNV parameters, the interference terms are neglected in our analysis. In the following, we extract the "on-axis" upper limits of these parameters using the most recent experimental half-lives lower

limits, as presented in Table I.

IV. EXPERIMENTAL LIMITS ON THE BSM LNV COUPLINGS

To obtain experimentally constrained upper limits of the effective LNV couplings one needs experimental half-life lower limits, accurate calculations of the PSF, together with reliable NME results calculated using nuclear structure methods tested to correctly describe the experimental nuclear structure data available for the nuclei involved. We split our analysis of the LNV parameters into three subsections corresponding the exchange of light left-handed Majorana neutrinos, the LNV couplings entering the remaining quark-level long-range diagrams, and the LNV couplings entering the quark-level short-range diagrams.

A. The exchange of light left-handed neutrinos

Most studies in the literature have considered just the case where only the exchange of light left-handed Majorana neutrinos contribute to the $0\nu\beta\beta$ decay process, presented in Figs. 1b and 2b. Therefore, one can easily find calculations of NME and PSF for this scenario. Considering this case, we reduce the half-life equation to:

$$\left[T_{1/2}^{0\nu} \right]^{-1} = g_A^4 |\eta_{0\nu}|^2 \mathcal{M}_{0\nu}^2, \quad (6)$$

where $g_A = 1.27$, $\mathcal{M}_{0\nu}^2$ contains the coefficients containing combinations of NME and PSF (see Eq. (8) below). $\eta_{0\nu} = \frac{\langle m_{\beta\beta} \rangle}{m_e}$, where m_e is the electron mass and $\langle m_{\beta\beta} \rangle$ represents the effective Majorana neutrino mass described as [66]:

$$\langle m_{\beta\beta} \rangle = \left| \sum_{j=1}^3 U_{ej}^2 m_j \right|. \quad (7)$$

Here U_{ej} are the PMNS mixing matrix elements [83, 84] and the summation is performed over all the three light neutrino mass eigenstates m_j . Also in Eq. (6)

$$\mathcal{M}_{0\nu}^2 = G_{01} \left[M_{GT} - \left(\frac{g_V}{g_A} \right)^2 M_F + M_T \right]^2, \quad (8)$$

where $g_V = 1$ is the vector coupling constant, $g_A = 1.27$ is the axial coupling constant, and G_{01} is the phase-space factor. The three NME, M_{GT} , M_F , and M_T (shown in Table IX) correspond to the Gamow-Teller, Fermi and Tensor transition operators, respectively, and are described in the Appendix. All the NME listed in the tables of the Appendix have the correct signs relative to that of M_{GT} , which is chosen to be positive. The \mathcal{M}^2 coefficients correctly include these relative signs, but the overall sign

TABLE III. The first line shows values of the $\mathcal{M}_{0\nu}^2$ coefficients containing combinations of NME and PSF, and the second line presents the extracted neutrino physics parameter $|\eta_{0\nu}|$ for the most studied case, assuming only the exchange of light left-handed Majorana neutrinos.

	^{48}Ca	^{76}Ge	^{82}Se	^{130}Te	^{136}Xe
$\mathcal{M}_{0\nu}^2 \cdot 10^{14}$	2.61	3.01	11.6	5.23	4.41
$ \eta_{0\nu} \cdot 10^6$	27.1	0.49	3.6	1.36	0.28

of the \mathcal{M} in Eqs. (8, 10, 12, 14, and 16) is lost due to squaring.

In Table III we present the $\mathcal{M}_{0\nu}^2$ values and their corresponding $\eta_{0\nu}$ limits. We find the lowest upper-limit of this parameter for ^{136}Xe , which leads to a limit for the Majorana neutrino mass $\langle m_{\beta\beta} \rangle \sim 140$ meV.

B. The long-range effective LNV couplings

Investigating the “on-axis” LNV parameters of the diagram of Fig. 2c, the half-life is factorized as:

$$\left[T_{1/2}^{0\nu} \right]^{-1} = g_A^4 \left[|\epsilon_\alpha^\beta|^2 \mathcal{M}_{\alpha\beta}^2 \right], \quad (9)$$

with $\epsilon_\alpha^\beta = \{\epsilon_{V-A}^{V+A}, \epsilon_{V+A}^{V+A}, \epsilon_{S\pm P}^{S+P}, \epsilon_{TL}^{TR}, \epsilon_{TR}^{TR}\}$. Here and below the $\alpha\beta$ combination corresponds to some index i in Eq. (5), as described in the definition of \mathcal{E}_i after Eq. (5). Following the formalism presented in Refs. [17, 19, 58] and including the $G_{01} - G_{09}$ PSF, we write the long-range coefficients containing combinations of NME and PSF as:

$$\mathcal{M}_{V+A/V-A}^2 = G_{02} \mathcal{M}_{2+}^2 - \frac{2}{9} G_{03} \mathcal{M}_{1-} \mathcal{M}_{2+} + \frac{1}{9} G_{04} \mathcal{M}_{1-}^2 - G_{07} M_P M_R + G_{08} M_P^2 + G_{09} M_R^2, \quad (10a)$$

$$\mathcal{M}_{V+A/V+A}^2 = G_{02} \mathcal{M}_{2-}^2 - \frac{2}{9} G_{03} \mathcal{M}_{1+} \mathcal{M}_{2-} + \frac{1}{9} G_{04} \mathcal{M}_{1+}^2, \quad (10b)$$

$$\text{with } \mathcal{M}_{1\pm} = M_{GTq} \pm 3 \left(\frac{g_V}{g_A} \right)^2 M_{Fq} - 6 M_{Tq}$$

$$\text{and } \mathcal{M}_{2\pm} = M_{GT\omega} \pm \left(\frac{g_V}{g_A} \right)^2 M_{F\omega} - \frac{1}{9} \mathcal{M}_{1\pm},$$

$$\mathcal{M}_{S+P/S\pm P}^2 = G_{01} \left[\frac{F_P^{(3)}}{R m_e g_A} \left(\frac{1}{3} M_{GT'} + M_{T'} \right) \right]^2, \quad (10c)$$

$$\begin{aligned} \mathcal{M}_{TR/TR}^2 &= G_{01} \left[\frac{4T_1^{(3)} g_V (1 - (\mu_p - \mu_n))}{R m_e g_A^2} \right. \\ &\quad \left. \times \left(M_{T'} - \frac{2}{3} M_{GT'} \right) \right]^2, \end{aligned} \quad (10d)$$

$$\mathcal{M}_{TR/TL}^2 = G_{01} \left[\frac{g_V (8\hat{T}_2^{(3)} - 4T_1^{(3)})}{R m_e g_A^2} M_{F'} \right]$$

$$- \frac{4T_1^{(3)} 2m_p}{g_A R^2 m_e m_\pi^2} \left(M_{T''} + \frac{1}{3} M_{GT''} \right) \right]^2. \quad (10e)$$

In these equations, $R = 1.2A^{1/3}$ fm is the nuclear radius, $m_e = 0.511$ MeV is the electron mass, $m_\pi = 139$ MeV is the pion mass, $m_p = 938$ MeV is the proton mass, $(\mu_p - \mu_n) \simeq 3.7$, and the parameters $F_P^{(3)} = 4.41$, $T_1^{(3)} = 1.38$, $\hat{T}_2^{(3)} = -4.54$ are taken from Ref. [85] where they have been calculated using the MIT bag model. Detailed expressions for the individual M_α (with $\alpha = GTq, Fq, Tq, GT\omega, F\omega, P, R, GT', F', T', GT'', T''$) are found in the Appendix.

It is possible to obtain another limit for $\tilde{\epsilon}_{TR}^{TR}$ by considering a different hadronization procedure [70] depicted in Fig. 2e, where our $\eta_{\pi\nu}$ plays the same role as $\eta_{(q)LR}^{11}$ in Eq.(22) of Ref. [70]. In this case we can obtain an alternative value for ϵ_{TR}^{TR} , $\tilde{\epsilon}_{TR}^{TR} = \eta_{\pi\nu}/8$.

$$\left[T_{1/2}^{0\nu} \right]^{-1} = g_A^4 \left[|8 \tilde{\epsilon}_{TR}^{TR}|^2 \mathcal{M}_{\pi\nu}^2 \right], \quad (11)$$

with

$$\mathcal{M}_{\pi\nu}^2 = G_{01} [M_{GT\pi\nu} + M_{T\pi\nu}]^2. \quad (12)$$

The $M_{GT\pi\nu}$ and $M_{T\pi\nu}$ are the same NME as $M_{GT(\bar{q})}$ and $M_{GT(\bar{q})}$ in Eq.(155) of Ref.[74] (also described in the Appendix).

TABLE IV. The $\mathcal{M}_{\alpha\beta}^2$ values for the long-range part of the $0\nu\beta\beta$ decay process.

	⁴⁸ Ca	⁷⁶ Ge	⁸² Se	¹³⁰ Te	¹³⁶ Xe
$10^9 \cdot \mathcal{M}_{V+A/V-A}^2$	1.49	1.44	5.24	3.76	3.17
$10^{13} \cdot \mathcal{M}_{V+A/V+A}^2$	1.09	0.39	3.21	1.11	0.89
$10^{10} \cdot \mathcal{M}_{S+P/S\pm P}^2$	1.62	1.17	4.20	4.73	4.18
$10^8 \cdot \mathcal{M}_{TR/TR}^2$	6.07	1.15	4.43	2.45	1.95
$10^7 \cdot \mathcal{M}_{TR/TL}^2$	3.42	0.25	0.80	1.74	1.59
$10^{10} \cdot \mathcal{M}_{\pi\nu}^2$	2.84	2.62	10.2	4.85	4.13

Table IV shows our shell model $\mathcal{M}_{\alpha\beta}^2$ coefficients. We present our values for the long-range LNV parameters in Table V, where $\tilde{\epsilon}_{TR}^{TR}$ represents the alternative limit for ϵ_{TR}^{TR} that is obtained using $\mathcal{M}_{\pi\nu}$. With the exception of ⁴⁸Ca, the $\tilde{\epsilon}_{TR}^{TR}$ upper-limits are slightly lower than those of ϵ_{TR}^{TR} .

The shell model values for M_α , with $\alpha = GTq, Fq, Tq, GT\omega, F\omega, P, R, GT', F', T', GT'', T''$, $GT\pi\nu, T\pi\nu$, are shown in Table X of the Appendix.

C. The short-range LNV couplings

Similar to the case of the long-range component, we extract the “on-axis” values of the short-range LNV parameters using the following expression for the half-life

TABLE V. The “on-axis” values of the long-range LNV parameters ϵ_α^β . The last two lines present $\eta_{\pi\nu}$ and its corresponding $\tilde{\epsilon}_{TR}^{TR}$ limit.

	⁴⁸ Ca	⁷⁶ Ge	⁸² Se	¹³⁰ Te	¹³⁶ Xe
$ \epsilon_{V-A}^{V+A} $	$1.1 \cdot 10^{-7}$	$2.2 \cdot 10^{-9}$	$1.7 \cdot 10^{-8}$	$5.1 \cdot 10^{-9}$	$1.1 \cdot 10^{-9}$
$ \epsilon_{V+A}^{V+A} $	$1.3 \cdot 10^{-5}$	$4.3 \cdot 10^{-7}$	$2.2 \cdot 10^{-6}$	$9.3 \cdot 10^{-7}$	$2.0 \cdot 10^{-7}$
$ \epsilon_{S\pm P}^{S+P} $	$3.4 \cdot 10^{-7}$	$7.9 \cdot 10^{-9}$	$6.1 \cdot 10^{-8}$	$1.4 \cdot 10^{-8}$	$2.9 \cdot 10^{-9}$
$ \epsilon_{TR}^{TR} $	$1.8 \cdot 10^{-8}$	$7.9 \cdot 10^{-10}$	$5.9 \cdot 10^{-9}$	$2.0 \cdot 10^{-9}$	$4.2 \cdot 10^{-10}$
$ \epsilon_{TL}^{TR} $	$7.5 \cdot 10^{-9}$	$5.4 \cdot 10^{-10}$	$4.4 \cdot 10^{-9}$	$7.4 \cdot 10^{-10}$	$1.5 \cdot 10^{-10}$
$ \eta_{\pi\nu} $	$2.6 \cdot 10^{-7}$	$5.3 \cdot 10^{-9}$	$3.9 \cdot 10^{-8}$	$1.4 \cdot 10^{-8}$	$2.9 \cdot 10^{-9}$
$ \tilde{\epsilon}_{TR}^{TR} $	$3.3 \cdot 10^{-8}$	$6.6 \cdot 10^{-10}$	$4.8 \cdot 10^{-9}$	$1.8 \cdot 10^{-9}$	$3.6 \cdot 10^{-10}$

corresponding to the diagram of Fig. 1d:

$$\left[T_{1/2}^{0\nu} \right]^{-1} = g_A^4 \left[|\epsilon_\alpha^\beta|^2 \mathcal{M}_{\alpha\beta}^2 \right], \quad (13)$$

with $\epsilon_\alpha^\beta = \{\epsilon_1, \epsilon_2, \epsilon_3^{LLz(RRz)}, \epsilon_3^{LRz(RLz)}, \epsilon_4, \epsilon_6\}$. The index $\beta = xyz$, with $xyz = L/R, L/R, L/R$, indicates the chirality of the hadronic and the leptonic currents. It is only possible to distinguish between the different chiralities in the case of ϵ_3 where we denote them explicitly as $\epsilon_3^{LLz(RRz)}$ and $\epsilon_3^{LRz(RLz)}$. For the other cases we omit this labeling.

Adapting the formalism of Ref. [18, 19, 74], we can write the coefficients containing combinations of NME and PSF as:

$$\mathcal{M}_1^2 = G_{01} \left[\left(\frac{F_S^{(3)}}{g_A} \right)^2 M_{FN} \right]^2, \quad (14a)$$

$$\mathcal{M}_2^2 = G_{01} \left[\left(8 \frac{T_1^{(3)}}{g_A} \right)^2 M_{GTN} \right]^2, \quad (14b)$$

$$\begin{aligned} \mathcal{M}_{3LLz}^2 &= \mathcal{M}_{3RRz}^2 \\ &= G_{01} \left[M_{GTN} - \left(\frac{g_V}{g_A} \right)^2 M_{FN} \right]^2, \end{aligned} \quad (14c)$$

$$\begin{aligned} \mathcal{M}_{3LRz}^2 &= \mathcal{M}_{3RLz}^2 \\ &= G_{01} \left[M_{GTN} + \left(\frac{g_V}{g_A} \right)^2 M_{FN} \right]^2, \end{aligned} \quad (14d)$$

$$\mathcal{M}_4^2 = G_{09} \frac{(m_e R)^2}{8} \left[\frac{T_1^{(3)}}{g_A} M_{GTN} \right]^2, \quad (14e)$$

$$\mathcal{M}_5^2 = G_{09} \frac{(m_e R)^2}{8} \left[\frac{F_S^{(3)} g_V}{g_A^2} M_{FN} \right]^2. \quad (14f)$$

The parameters $F_S^{(3)} = 0.48$ and $T_1^{(3)} = 1.38$ are taken from Ref. [85]. The values of these $\mathcal{M}_{\alpha\beta}^2$ are presented in Table VI. Detailed expressions for M_{GTN} and M_{FN} are presented in the Appendix, and their shell model values are shown in Table XI.

TABLE VI. The $\mathcal{M}_{\alpha\beta}^2$ values for the short-range LNV parameters.

	^{48}Ca	^{76}Ge	^{82}Se	^{130}Te	^{136}Xe
$10^{13} \cdot \mathcal{M}_1^2$	2.63	1.83	6.86	4.83	4.03
$10^8 \cdot \mathcal{M}_2^2$	0.75	0.54	2.00	1.46	1.21
$10^{10} \cdot \mathcal{M}_{3LLz(RRz)}^2$	1.30	0.92	3.45	2.50	2.07
$10^{11} \cdot \mathcal{M}_{3LRz(RLz)}^2$	4.82	3.48	13.0	9.54	7.87
$10^{10} \cdot \mathcal{M}_4^2$	1.00	0.75	2.68	1.89	1.56
$10^{12} \cdot \mathcal{M}_5^2$	1.15	0.84	3.01	2.06	1.72
$10^9 \cdot \mathcal{M}_{\pi N}^2$	3.36	0.87	3.24	2.43	1.94

Considering the $0\nu\beta\beta$ amplitudes displayed in Figs. 2f and 2g in the one-pion and two-pion exchange modes it is possible to get alternative limits for ε_1 and ε_2 considering a different coefficient, $\mathcal{M}_{\pi N}$. The analysis of Ref. [78] suggests these alternative values, here denoted by $\tilde{\varepsilon}_1$ and $\tilde{\varepsilon}_2$, can be obtained as $\tilde{\varepsilon}_1 = \frac{64}{16} \eta_{\pi N}$, and $\tilde{\varepsilon}_2 = \frac{2}{3} \eta_{\pi N}$, using

$$\left[T_{1/2}^{0\nu} \right]^{-1} = g_A^4 \left[|\eta_{\pi N}|^2 \mathcal{M}_{\pi N}^2 \right], \quad (15)$$

where

$$\begin{aligned} \mathcal{M}_{\pi N}^2 = G_{01} & \left[c^{1\pi} (M_{GT1\pi} + M_{T1\pi}) \right. \\ & \left. + c^{2\pi} (M_{GT2\pi} + M_{T2\pi}) \right]^2. \end{aligned} \quad (16)$$

The expressions for the factors $c^{1\pi}$ and $c^{2\pi}$ are found in Eq. (151) of Ref. [74]. These factors depend on the masses of the up and down quark, and choosing $(m_u + m_d) = 11.6$ MeV [27, 86], one gets $c^{1\pi} = -83.598$, $c^{2\pi} = 359.436$ that we use in these calculations. The description of M_α (with $\alpha = GT1\pi, T1\pi, GT2\pi, T2\pi$) is presented in the Appendix.

Shown in Table VII are the values of the short-range LNV parameters. Using the different hadronization presented in Figs. 2f and 2g, $\tilde{\varepsilon}_1$ provides significantly more stringent upper-limits than ε_1 . With the exception of ^{48}Ca , where the $\tilde{\varepsilon}_2$ limit is identical to ε_2 , the other $\tilde{\varepsilon}_2$ upper-limits are almost double those of ε_2 . Therefore, we conclude that ε_2 are better constrained.

V. DISCUSSIONS

From the $\eta_{0\nu}$ limits presented in Table III for ^{136}Xe , one gets the lowest shell model upper-limit for the Majorana neutrino mass $\langle m_{\beta\beta} \rangle \sim 140$ meV. A wider range of values, 60 – 165 meV can be found if the NME calculated with a larger number of nuclear models are considered [64].

Considering the diagram in Fig. 2e, it is possible to get lower limits for ϵ_{TR}^{TR} , denoted as $\tilde{\epsilon}_{TR}^{TR}$ in Table V, than those corresponding to the diagram in Fig. 2c, with the exception of ^{48}Ca , as can be seen in Table V. Considering the different hadronization scenario presented in Figs. 2f

TABLE VII. The “on-axis” values of the short-range LNV parameters ε_α^β . The last three lines present the $\eta_{\pi N}$ limits for \mathcal{R}_p SUSY, and their corresponding $\tilde{\varepsilon}_1$ and $\tilde{\varepsilon}_1$ limits, respectively.

	^{48}Ca	^{76}Ge	^{82}Se	^{130}Te	^{136}Xe
$ \varepsilon_1 $	$8.6 \cdot 10^{-6}$	$2.0 \cdot 10^{-7}$	$1.5 \cdot 10^{-6}$	$4.5 \cdot 10^{-7}$	$9.3 \cdot 10^{-8}$
$ \varepsilon_2 $	$5.1 \cdot 10^{-8}$	$1.2 \cdot 10^{-9}$	$8.8 \cdot 10^{-9}$	$2.6 \cdot 10^{-9}$	$5.4 \cdot 10^{-10}$
$ \varepsilon_3^{LLz(RRz)} $	$3.8 \cdot 10^{-7}$	$8.9 \cdot 10^{-9}$	$6.7 \cdot 10^{-8}$	$2.0 \cdot 10^{-8}$	$4.1 \cdot 10^{-9}$
$ \varepsilon_3^{LRz(RLz)} $	$6.3 \cdot 10^{-7}$	$1.4 \cdot 10^{-8}$	$1.1 \cdot 10^{-7}$	$3.2 \cdot 10^{-8}$	$6.7 \cdot 10^{-9}$
$ \varepsilon_4 $	$4.4 \cdot 10^{-7}$	$9.8 \cdot 10^{-9}$	$7.6 \cdot 10^{-8}$	$2.3 \cdot 10^{-8}$	$4.7 \cdot 10^{-9}$
$ \varepsilon_5 $	$4.1 \cdot 10^{-6}$	$9.3 \cdot 10^{-8}$	$7.1 \cdot 10^{-7}$	$2.2 \cdot 10^{-7}$	$4.5 \cdot 10^{-8}$
$ \eta_{\pi N} $	$7.6 \cdot 10^{-8}$	$2.9 \cdot 10^{-9}$	$2.2 \cdot 10^{-8}$	$6.3 \cdot 10^{-9}$	$1.3 \cdot 10^{-9}$
$ \tilde{\varepsilon}_1 $	$3.2 \cdot 10^{-7}$	$1.2 \cdot 10^{-8}$	$9.3 \cdot 10^{-8}$	$2.7 \cdot 10^{-8}$	$5.7 \cdot 10^{-9}$
$ \tilde{\varepsilon}_2 $	$5.0 \cdot 10^{-8}$	$1.9 \cdot 10^{-9}$	$1.5 \cdot 10^{-8}$	$4.2 \cdot 10^{-9}$	$8.9 \cdot 10^{-10}$

TABLE VIII. The BSM effective scale (in GeV) for different dimension-D operators at the present ^{136}Xe half-life limit (Λ_D^0) and for $T_{1/2} \approx 1.1 \times 10^{28}$ years (Λ_D).

\mathcal{O}_D	$\bar{\epsilon}_D$	$\Lambda_D^0(y=1)$	$\Lambda_D^0(y=y_e)$	$\Lambda_D(y=y_e)$
\mathcal{O}_5	$2.8 \cdot 10^{-7}$	$2.12 \cdot 10^{14}$		1904
\mathcal{O}_7	$2.0 \cdot 10^{-7}$	$3.76 \cdot 10^4$		542
\mathcal{O}_9	$9.3 \cdot 10^{-8}$	$2.72 \cdot 10^3$		2718
\mathcal{O}_{11}	$9.3 \cdot 10^{-8}$	$1.24 \cdot 10^3$	33	46

and 2g, $\tilde{\varepsilon}_1$ provides a significantly more stringent upper-limits than ε_1 . With the exception of ^{48}Ca , where the $\tilde{\varepsilon}_2$ limit is identical to ε_2 , the other $\tilde{\varepsilon}_2$ upper-limits are almost double those of ε_2 .

As suggested in Ref. [81] (see the diagrams of their Fig.1), at the electroweak scale when the appropriate Higgs fields are included, the diagram 1.b originates from a dimension-5 BSM Lagrangian, \mathcal{O}_5 , responsible for the Majorana neutrino mass. Similarly the low-energy dimension-6 Lagrangian \mathcal{L}_6 corresponds to a dimension-7 BSM operator, \mathcal{O}_7 , and the low energy dimension-9 Lagrangian \mathcal{L}_9 can be rearranged as dimension-9 and dimension-11 operators, \mathcal{O}_9 and \mathcal{O}_{11} . Using the effective field theory one can infer the energy scale Λ_D up to which these effective field operators are not broken:

$$\mathcal{L}_D = \frac{g}{(\Lambda_D)^{D-4}} \mathcal{O}_D, \quad (17)$$

where D is the dimension of the effective field operator. Here g is considered to be a dimensionless coupling constant of the order of 1. Following Ref. [81] one can find relations between the constants entering our \mathcal{L}_6 and \mathcal{L}_9 Lagrangian and the effective field theory Lagrangians above the electroweak scale, Eq. (17).

$$\begin{aligned} m_e \bar{\epsilon}_5 &= \frac{g^2(yv)^2}{\Lambda_5}, & \frac{G_F \bar{\epsilon}_7}{\sqrt{2}} &= \frac{g^3(yv)}{2(\Lambda_7)^3}, \\ \frac{G_F^2 \bar{\epsilon}_9}{2m_p} &= \frac{g^4}{(\Lambda_9)^5}, & \frac{G_F^2 \bar{\epsilon}_{11}}{2m_p} &= \frac{g^6(yv)^2}{(\Lambda_{11})^7}. \end{aligned} \quad (18)$$

Here, $m_e = 0.511 \times 10^{-3}$ GeV is the electron mass, $g = 1$ is a generic coupling constant, $v = 174$ GeV is the Higgs vacuum expectation value, y is a Yukawa coupling associated to the interaction with the Higgs bosons, $G_F = 1.166 \times 10^{-5}$ GeV $^{-2}$ is the Fermi coupling constant, and $m_p = 0.938$ GeV is the proton mass. The $\bar{\epsilon}_D$ (with $D = \{5, 7, 9, 11\}$) can be extracted from the LNV parameters in Eqs. (2) and (3). Considering that values of these LNV parameters may be affected by mixing angles that might distort the scales in Eq. (17), we choose their maximum values: $\bar{\epsilon}_5 = |\eta_{0\nu}|$, $\bar{\epsilon}_7 = \text{Max} \left[|\epsilon_{V-A}^{V+A}|, |\epsilon_{V+A}^{V+A}|, |\epsilon_{S\pm P}^{S+P}|, |\epsilon_{TL}^{TR}|, |\epsilon_{TR}^{TR}| \right]$, $\bar{\epsilon}_9 = \text{Max} \left[|\varepsilon_1|, |\varepsilon_2|, |\varepsilon_3^{LLz(RRz)}|, |\varepsilon_3^{LRz(RLz)}|, |\varepsilon_4|, |\varepsilon_5| \right]$, and $\bar{\epsilon}_{11} = \bar{\epsilon}_9$.

To extract the limits of the BSM scales $\Lambda_{5,7,9,11}$ we need the most stringent limits for the LNV parameters, which are found for the case of ^{136}Xe . Inspecting Tables V and VII we found that $\bar{\epsilon}_5$ corresponds to the $\eta_{0\nu}$ parameter of the light left-handed Majorana neutrino exchange mechanism. For $\bar{\epsilon}_7$ we choose ϵ_{V+A}^{V+A} , that is the largest long-range ϵ_α^β parameter. In the case of $\bar{\epsilon}_9 = \bar{\epsilon}_{11}$ we select ε_1 , being the largest short-range ε_α^β parameter. These values are listed in Table VIII.

As in Ref. [81] we take $g = 1$ in Eq. (17). However, we introduce here the Yukawa coupling y between the Higgs boson field and the fermion fields, and we consider two cases: (i) $y = 1$ corresponding to the top quark mass (choice made in Ref. [81]), and (ii) $y = 3 \times 10^{-6}$ corresponding to the electron mass. Based on these values we calculate the limits of the new BSM scales or different dimension-D operators. The results are shown in Table VIII. The Λ_D^0 scales are calculated using the present lower limit for the half-life of ^{136}Xe , 1.1×10^{26} . Λ_D is estimated assuming a half-life of $T_{1/2} \approx 1.1 \times 10^{28}$ years, which would correspond to a $\langle m_{\beta\beta} \rangle \approx 14$ meV.

The Λ_9 scale does not depend on the unknown Yukawa coupling, and from that point of view, if \mathcal{O}_9 amplitude is dominant, that would indicate that the scale of new physics should be found around 3 TeV. Unfortunately, the Λ_9 scale, as well as all other high D scales, are not very sensitive to the $0\nu\beta\beta$ half-life, because they scale as $T_{1/2}^{\frac{1}{2(D-4)}}$. \mathcal{O}_7 and \mathcal{O}_{11} provide small low-limits for Λ_7 and Λ_{11} . This feature is likely related to the fact that these terms are originating from small term in the mixing matrix (e.g. the small S matrix in Eq. (A3) of [11]), and thus $g \sim 1$ in Eq. (17) is not a good choice. The most sensitive scale to both the unknown Yukawa and the $0\nu\beta\beta$ half-life is Λ_5 . Assuming a Yukawa coupling corresponding to the electron mass, one can conclude that the $0\nu\beta\beta$ decay could be consistent with a new physics scale somewhere between 2 TeV and 20 TeV.

VI. CONCLUSIONS

This work advances and extends the analysis of BSM physics parameters involved in the neutrinoless double-beta decay. We calculate 23 nuclear matrix elements and 9 phase-space factors. Five of these nuclear matrix elements ($M_{GT'}$, $M_{GT''}$, $M_{F'}$, $M_{T'}$, and $M_{T''}$) are calculated for the first time using shell model techniques. Three new hadron-level diagrams, Fig. 2.e, 2.f, 2.g are for the first time considered in the full analyses based on the effective field theory approach to $0\nu\beta\beta$ decay (they were only considered in the past in the context of particular mechanisms).

Using a general effective field theory and assuming that one LNV coupling plays a dominant contribution to the $0\nu\beta\beta$ decay amplitude, we extract limits for the effective Majorana mass and 11 effective low-energy couplings in the case of five nuclei of immediate experimental interest. Due to the better half-life limits, the most stringent limits for the LNV couplings are found for ^{136}Xe , closely followed by ^{76}Ge . An upper-limit for the Majorana neutrino mass $\langle m_{\beta\beta} \rangle$ of 140 meV was calculated in the case of ^{136}Xe . Assuming a Yukawa coupling corresponding to the electron mass, one can conclude that the $0\nu\beta\beta$ decay could be consistent with a new physics scale somewhere between 2 TeV and 20 TeV.

Using the upper limits for the LNV coupling we extract limits for the energy scale of the new physics, using EFT arguments. We found that the scale associated with the dimension-9 EFT operator is stable, and indicates a new physics scale around 3 TeV. We also found that the dimension-5 EFT operator associated with the Majorana neutrino mass varies significantly with the Yukawa coupling to Higgs and the $0\nu\beta\beta$ decay half-life.

Should neutrinoless double-beta decay be experimentally observed, a thorough analysis of the outgoing electrons angular and energy distributions (presented in Ref. [11]) based on accurate calculations of the nuclear matrix elements is needed to investigate subsets of these LNV couplings and identify the presence of the right-handed currents.

VII. APPENDIX

In this Appendix, we present the detailed expressions for the \mathcal{M}_i^2 coefficients that are needed to analyze the outcome of Eq. (5).

The NME that enter the equations (8, 10, 12, 14, and 16) are written as a product of two-body transition densities (TBTD) and two-body matrix elements (TBME), where the summation is over all the nucleon states. Their numerical values when calculated within the shell model approach are presented in Table IX for the light left-handed Majorana neutrino exchange, in Table X for the long-range part in Fig. 2, and in Table XI for the short-range component of Fig. 2. The general

TABLE IX. NME values for the exchange of light left-handed Majorana neutrinos corresponding to the diagram in Fig. 2b.

	^{48}Ca	^{76}Ge	^{82}Se	^{130}Te	^{136}Xe
M_{GT}	0.807	3.206	3.005	1.662	1.505
M_F	-0.233	-0.674	-0.632	-0.438	-0.400
M_T	0.080	0.011	0.012	-0.007	-0.008

TABLE X. NME for the long-range part shown in Figs. 2c and 2e.

	^{48}Ca	^{76}Ge	^{82}Se	^{130}Te	^{136}Xe
M_{GTq}	0.709	3.228	3.034	1.587	1.440
$M_{GT\omega}$	0.930	3.501	3.287	1.855	1.682
$M_{GT'}$	0.841	2.699	2.567	2.120	1.935
$M_{GT''}$	3.581	11.982	11.490	12.210	11.202
$M_{GT\pi\nu}$	86.2	331.6	313.3	184.2	167.7
M_{Fq}	-0.121	-0.383	-0.362	-0.249	-0.230
$M_{F\omega}$	-0.232	-0.659	-0.618	-0.427	-0.391
$M_{F'}$	-0.258	-0.812	-0.772	-0.635	-0.581
M_{Tq}	-0.173	-0.059	-0.058	-0.013	-0.012
$M_{T'}$	0.337	0.015	0.025	-0.077	-0.085
$M_{T''}$	2.231	0.028	0.118	-0.773	-0.861
$M_{T\pi\nu}$	21.3	7.3	6.9	1.2	1.1
M_P	0.395	-2.466	-2.332	-1.729	-1.617
M_R	1.014	3.284	3.127	2.562	2.341

expressions for the NME are (see Refs. [11, 27, 58]):

$$M_\alpha = \sum_{j_p j_{p'} j_n j_{n'} J^\pi} TBTD(j_p j_{p'}, j_n j_{n'}; J^\pi) \times \left\langle j_p j_{p'}; J^\pi \left| \tau_{-1} \tau_{-2} \mathcal{O}_{12}^{\gamma, \phi, \theta, P, R} \right| j_n j_{n'}; J^\pi \right\rangle. \quad (19)$$

We group the operators that share similar structure into five families.

$$\begin{aligned} \text{Gamow-Teller operator : } & \mathcal{O}_{12}^\gamma = \vec{\sigma}_1 \cdot \vec{\sigma}_2 H_\gamma(r), \\ \text{Fermi operator : } & \mathcal{O}_{12}^\phi = H_\phi(r), \\ \text{Tensor operator : } & \mathcal{O}_{12}^\theta = [3(\vec{\sigma}_1 \cdot \hat{\mathbf{r}})(\vec{\sigma}_2 \cdot \hat{\mathbf{r}}) - \vec{\sigma}_1 \cdot \vec{\sigma}_2] H_\theta(r), \\ \text{P operator : } & \mathcal{O}_{12}^P = (\vec{\sigma}_1 - \vec{\sigma}_2) H_P(r), \\ \text{R operator : } & \mathcal{O}_{12}^R = \vec{\sigma}_1 \cdot \vec{\sigma}_2 H_R(r). \end{aligned}$$

Here, $\gamma = GT, GT\omega, GTq, GTN, GT', GT'', GT\pi\nu, GT1\pi, GT2\pi$, $\phi = F, F\omega, Fq, FN, F'$, and $\theta = T, Tq, T', T'', T\pi\nu, T1\pi, T2\pi$. Equations (20) present the radial part of the NME and their expressions are adapted for consistency from Refs. [58], [19], and [74].

$$H_{GT} = \frac{2R}{\pi} \int \frac{h_A^2(q^2)}{q(q + \bar{E})} j_0(qr) q^2 dq, \quad (20a)$$

$$H_{GT\omega} = \frac{2R}{\pi} \int \frac{h_A^2(q^2)}{(q + \bar{E})^2} j_0(qr) q^2 dq, \quad (20b)$$

$$H_{GTq} = \frac{2R}{\pi} r \int \frac{h_A^2(q^2)}{q + \bar{E}} j_1(qr) q^2 dq, \quad (20c)$$

TABLE XI. The short-range NME involved in Figs. 2d, 2f, and 2g.

	^{48}Ca	^{76}Ge	^{82}Se	^{130}Te	^{136}Xe
M_{GTN}	58.5	162.3	150.1	107.6	96.6
$M_{GT1\pi}$	-1.354	-3.559	-3.282	-2.421	-2.171
$M_{GT2\pi}$	-0.676	-1.983	-1.854	-1.257	-1.136
M_{FN}	-22.9	-62.6	-58.1	-41.0	-36.9
$M_{T1\pi}$	-0.590	-0.010	-0.027	0.106	0.115
$M_{T2\pi}$	-0.227	-0.010	-0.015	0.038	0.040

$$H_{GTN} = \frac{2R}{\pi m_e m_p} \int h_A^2(q^2) j_0(qr) q^2 dq, \quad (20d)$$

$$H_{GT'} = \frac{2R^2}{\pi m_p} \int \frac{q^2 h_A^2(q^2)}{q(q + \bar{E})} j_0(qr) q^2 dq, \quad (20e)$$

$$H_{GT''} = \frac{2R^3}{\pi m_p} \int \frac{q^2 h_A^2(q^2)}{q + \bar{E}} j_0(qr) q^2 dq, \quad (20f)$$

$$H_{GT\pi\nu} = \frac{2R}{\pi} \int \frac{h_{GT\pi\nu}^2(q^2)}{q(q + \bar{E})} j_0(qr) q^2 dq, \quad (20g)$$

$$H_{GT1\pi} = -\frac{2R}{\pi} \int h_A^2(q^2) \frac{q^2/m_\pi^4}{1 + q^2/m_\pi^2} j_0(qr) q^2 dq, \quad (20h)$$

$$H_{GT2\pi} = -\frac{4R}{\pi} \int h_A^2(q^2) \frac{q^2/m_\pi^4}{(1 + q^2/m_\pi^2)^2} j_0(qr) q^2 dq, \quad (20i)$$

$$H_F = \frac{2R}{\pi} \int \frac{h_V^2(q^2)}{q(q + \bar{E})} j_0(qr) q^2 dq, \quad (20j)$$

$$H_{F\omega} = \frac{2R}{\pi} \int \frac{h_V^2(q^2)}{(q + \bar{E})^2} j_0(qr) q^2 dq, \quad (20k)$$

$$H_{Fq} = \frac{2R}{\pi} r \int \frac{h_V^2(q^2)}{q + \bar{E}} j_1(qr) q^2 dq, \quad (20l)$$

$$H_{FN} = \frac{2R}{\pi m_e m_p} \int h_V^2(q^2) j_0(qr) q^2 dq, \quad (20m)$$

$$H_{F'} = \frac{2R^2}{\pi m_p} \int \frac{q^2 h_V^2(q^2)}{q(q + \bar{E})} j_0(qr) q^2 dq, \quad (20n)$$

$$H_T = -\frac{2R}{\pi} \int \frac{h_T^2(q^2)}{q(q + \bar{E})} j_2(qr) q^2 dq, \quad (20o)$$

$$H_{Tq} = \frac{2R}{3\pi} \sqrt{\frac{2}{3}} r C^{(2)}(\hat{\mathbf{r}}) \int \frac{h_A^2(q^2)}{q + \bar{E}} j_1(qr) q^2 dq, \quad (20p)$$

$$H_{T'} = -\frac{2R^2}{\pi m_p} \int \frac{q^2 h_A^2(q^2)}{q(q + \bar{E})} j_2(qr) q^2 dq, \quad (20q)$$

$$H_{T''} = -\frac{2R^3}{\pi m_p} \int \frac{q^2 h_A^2(q^2)}{q + \bar{E}} j_2(qr) q^2 dq, \quad (20r)$$

$$H_{T\pi\nu} = -\frac{2R}{\pi} \int \frac{h_{T\pi\nu}^2(q^2)}{q(q + \bar{E})} j_2(qr) q^2 dq, \quad (20s)$$

$$H_{T1\pi} = \frac{2R}{\pi} \int h_A^2(q^2) \frac{q^2/m_\pi^4}{1 + q^2/m_\pi^2} j_2(qr) q^2 dq, \quad (20t)$$

$$H_{T2\pi} = \frac{4R}{\pi} \int h_A^2(q^2) \frac{q^2/m_\pi^4}{(1 + q^2/m_\pi^2)^2} j_2(qr) q^2 dq, \quad (20u)$$

$$H_R = \frac{(\mu_p - \mu_n)}{3} \frac{g_V}{g_A} \frac{2R^2}{\pi m_p} \times \int q \frac{h_A(q^2)h_V(q^2)}{q + \bar{E}} j_0(qr) q^2 dq, \quad (20v)$$

$$H_P = \sqrt{2} \frac{2R}{\pi} \frac{g_V}{g_A} C^{(1)}(\hat{\mathbf{r}}) C^{(1)}(\hat{\mathbf{r}}_+) r_+ \times \int \frac{h_A(q^2)h_V(q^2)}{q + \bar{E}} j_1(qr) q^2 dq, \quad (20w)$$

Here, the expressions of $C_M^{(L)}$ and \mathbf{r} of Eqs. (20p, 20w) are:

$$C_M^{(L)} = \sqrt{\frac{4\pi}{2L+1}} Y_{LM},$$

$$\begin{aligned} \mathbf{r} &= \mathbf{r}_1 - \mathbf{r}_2, & \mathbf{r}_+ &= \frac{\mathbf{r}_1 + \mathbf{r}_2}{2}, & r &= |\mathbf{r}|, \\ \hat{\mathbf{r}} &= \frac{\mathbf{r}}{r}, & r_+ &= |\mathbf{r}_+|, & \hat{\mathbf{r}}_+ &= \frac{\mathbf{r}_+}{r_+}. \end{aligned}$$

The finite-size effects are taken into account via the following dipole form-factors:

$$g_A(q^2) = \left(\frac{\lambda_A^2}{\lambda_A^2 + q^2} \right)^2, \quad (21a)$$

$$g_V(q^2) = \left(\frac{\lambda_V^2}{\lambda_V^2 + q^2} \right)^2, \quad (21b)$$

$$g_M(q^2) = (\mu_p - \mu_n) g_V(q^2). \quad (21c)$$

Here $\lambda_A = 1086$ MeV and $\lambda_V = 850$ MeV are the axial and vector momentum cutoffs, respectively, and $(\mu_p - \mu_n) \simeq 3.7$.

The form-factors entering Eqs. 20 are:

$$h_V(q^2) = g_V(q^2), \quad (22a)$$

$$h_A(q^2) = g_A(q^2), \quad (22b)$$

$$h_{GT}^2(q^2) = g_A^2(q^2) \left[1 - \frac{2}{3} \frac{q^2}{q^2 + m_\pi^2} + \frac{1}{3} \left(\frac{q^2}{q^2 + m_\pi^2} \right)^2 \right] + \frac{2}{3} \frac{g_M^2(q^2)}{g_A^2} \frac{q^2}{4m_p^2}, \quad (22c)$$

$$h_T^2(q^2) = g_A^2(q^2) \left[\frac{2}{3} \frac{q^2}{q^2 + m_\pi^2} - \frac{1}{3} \left(\frac{q^2}{q^2 + m_\pi^2} \right)^2 \right] + \frac{1}{3} \frac{g_M^2(q^2)}{g_A^2} \frac{q^2}{4m_p^2}, \quad (22d)$$

$$h_{GT\pi\nu}^2(q^2) = -\frac{g_A^2(q^2)}{6} \frac{m_\pi^4}{m_e(m_u + m_d)} \frac{q^2}{(q^2 + m_\pi^2)^2}, \quad (22e)$$

$$h_{T\pi\nu}^2(q^2) = h_{GT\pi\nu}^2(q^2). \quad (22f)$$

$m_e = 0.511$ MeV is the electron mass, $m_\pi = 139$ MeV is the pion mass, $m_p = 938$ MeV is the proton mass, and the quark masses sum is $(m_u + m_d) = 11.6$ MeV [27, 86].

The NME presented in this section (Eq. (19)) are calculated using shell model approaches. To take into account the two-nucleon short-range correlation (SRC) we multiply the the relative wave functions by $f(r) = 1 - ce^{-ar^2}(1 - br^2)$; in the CD-Bonn parametrization used here $a = 1.52$ fm $^{-2}$, $b = 1.88$ fm $^{-2}$, and $c = 0.46$ fm $^{-2}$ [87]. This method is described in greater detail in Refs. [27, 32–37, 39–42]. The signs of all the NME presented in the following tables are relative to the sign of M_{GT} , which is taken to be positive. Table IX presents the M_{GT} , M_F , and M_T NME involved in the standard mass mechanism with left-handed currents of Eq. (8). For these NME, an optimal closure energy $\langle \bar{E} \rangle$ was used for each effective Hamiltonian [36]: $\langle \bar{E} \rangle = 0.5$ MeV for ^{48}Ca [34] and the GXPF1A Hamiltonian [88], $\langle \bar{E} \rangle = 3.4$ MeV for ^{76}Ge [56] and ^{82}Se [36] calculated with the JUN45 Hamiltonian [89], and $\langle \bar{E} \rangle = 3.5$ MeV for ^{130}Te [40] and ^{136}Xe [35] calculated with the SVD Hamiltonian [90].

The long-range NME M_α (with $\alpha = GTq$, Fq , Tq , $GT\omega$, $F\omega$, P , R , GT' , F' , T' , GT'' , T'') that appear in Eq. (10) and $M_{GT\pi\nu}$ and $M_{T\pi\nu}$ of Eq. (12) are presented in Table X.

Shown in Table XI are the short-range NME M_{GTN} and M_{FN} that appear in Eq. (14) and M_α (with $\alpha = GT1\pi$, $T1\pi$, $GT2\pi$, $T2\pi$) in Eq. 16).

VIII. ACKNOWLEDGMENTS

Support from the NUCLEI SciDAC Collaboration under U.S. Department of Energy Grant No. de-sc0008529 is acknowledged. M. Horoi also acknowledges the U.S. NSF Grant No. PHY-1404442 and the U.S. Department of Energy Grant No. de-sc0015376.

[1] J. Schechter and J. W. F. Valle, Phys. Rev. D **25**, 2951 (1982).
[2] J. Nieves, Phys. Lett. B **147**, 375 (1984).
[3] E. Takasugi, Phys. Lett. B **149**, 372 (1984).
[4] M. Hirsch, S. Kovalenko, and I. Schmidt, Phys. Lett. B **642**, 106 (2006).
[5] J. Pati and A. Salam, Phys. Rev. D **10**, 275 (1974).
[6] R. Mohapatra and J. Pati, Phys. Rev. D **11**, 2558 (1975).
[7] G. Senjanovic and R. N. Mohapatra, Phys. Rev. D **12**, 1502 (1975).
[8] W.-Y. Keung and G. Senjanovic, Phys. Rev. Lett. **50**, 1427 (1983).

[9] J. Barry and W. Rodejohann, *J. High Energy Phys.* p. 153 (2013).

[10] V. Khachatryan, A. M. Sirunyan, A. Tumasyan, W. Adam, T. Bergauer, M. Dragicevic, J. Er, C. Fabjan, M. Friedl, R. Fruhwirth, et al. (CMS-Collaboration), *Eur. Phys. J. C* **74**, 3149 (2014).

[11] M. Horoi and A. Neacsu, *Phys. Rev. D* **93**, 113014 (2016), arXiv:1511.00670 [hep-ph].

[12] A. Neacsu and M. Horoi, *Advances in High Energy Physics* **2016** (2016).

[13] V. Cirigliano, W. Dekens, J. de Vries, M. L. Graesser, and E. Mereghetti (2017), arXiv:1708.09390.

[14] V. Cirigliano, W. Dekens, M. Graesser, and E. Mereghetti, *Physics Letters B* **769**, 460 (2017), ISSN 0370-2693, URL <http://www.sciencedirect.com/science/article/pii/S0370269317302940>.

[15] E. Berkowitz, D. Brantley, C. Bouchard, C. C. Chang, M. A. Clark, N. Garron, B. Joo, T. Kurth, C. Monahan, H. Monge-Camacho, et al. (2017), arXiv:1704.01114.

[16] M. Hirsch, H. V. Klapdor-Kleingrothaus, and S. G. Kovalenko, *Phys. Lett. B* **372**, 181 (1996), hep-ph/9512237.

[17] H. Pas, M. Hirsch, H. V. Klapdor-Kleingrothaus, and S. G. Kovalenko, *Phys. Lett. B* **453**, 194 (1999).

[18] H. Pas, M. Hirsch, H. V. Klapdor-Kleingrothaus, and S. G. Kovalenko, *Phys. Lett. B* **498**, 35 (2001), hep-ph/0008182.

[19] F. F. Deppisch, M. Hirsch, and H. Pas, *J. Phys. G* **39**, 124007 (2012).

[20] F. Simkovic, G. Pantis, J. D. Vergados, and A. Faessler, *Phys. Rev. C* **60**, 055502 (1999).

[21] J. Suhonen and O. Civitarese, *Nucl. Phys. A* **847**, 207 (2010).

[22] A. Faessler, A. Meroni, S. T. Petcov, F. Simkovic, and J. Vergados, *Phys. Rev. D* **83**, 113003 (2011).

[23] M. T. Mustonen and J. Engel, *Phys. Rev. C* **87**, 064302 (2013).

[24] A. Faessler, M. Gonzalez, S. Kovalenko, and F. Simkovic, *Phys. Rev. D* **90**, 096010 (2014).

[25] J. Retamosa, E. Caurier, and F. Nowacki, *Phys. Rev. C* **51**, 371 (1995).

[26] E. Caurier, F. Nowacki, A. Poves, and J. Retamosa, *Phys. Rev. Lett.* **77**, 1954 (1996).

[27] M. Horoi, *Phys. Rev. C* **87**, 014320 (2013).

[28] A. Neacsu and S. Stoica, *Advances in High Energy Physics* **2014** (2014).

[29] E. Caurier, J. Menendez, F. Nowacki, and A. Poves, *Phys. Rev. Lett.* **100**, 052503 (2008).

[30] J. Menendez, A. Poves, E. Caurier, and F. Nowacki, *Nucl. Phys. A* **818**, 139 (2009).

[31] E. Caurier, G. Martinez-Pinedo, F. Nowacki, A. Poves, and A. P. Zuker, *Rev. Mod. Phys.* **77**, 427 (2005).

[32] M. Horoi and S. Stoica, *Phys. Rev. C* **81**, 024321 (2010).

[33] A. Neacsu, S. Stoica, and M. Horoi, *Phys. Rev. C* **86**, 067304 (2012).

[34] R. A. Sen'kov and M. Horoi, *Phys. Rev. C* **88**, 064312 (2013).

[35] M. Horoi and B. A. Brown, *Phys. Rev. Lett.* **110**, 222502 (2013).

[36] R. A. Sen'kov, M. Horoi, and B. A. Brown, *Phys. Rev. C* **89**, 054304 (2014).

[37] B. A. Brown, M. Horoi, and R. A. Sen'kov, *Phys. Rev. Lett.* **113**, 262501 (2014).

[38] A. Neacsu and S. Stoica, *J. Phys. G* **41**, 015201 (2014).

[39] R. A. Sen'kov and M. Horoi, *Phys. Rev. C* **90**, 051301(R) (2014).

[40] A. Neacsu and M. Horoi, *Phys. Rev. C* **91**, 024309 (2015).

[41] M. Horoi and A. Neacsu, *Phys. Rev. C* **93**, 024308 (2016).

[42] M. Horoi, S. Stoica, and B. A. Brown, *Phys. Rev. C* **75**, 034303 (2007).

[43] M. Blennow, E. Fernandez-Martinez, J. Lopez-Pavon, and J. Menendez, *JHEP* **07**, 096 (2010).

[44] J. Barea and F. Iachello, *Phys. Rev. C* **79**, 044301 (2009).

[45] J. Barea, J. Kotila, and F. Iachello, *Phys. Rev. Lett.* **109**, 042501 (2012).

[46] J. Barea, J. Kotila, and F. Iachello, *Phys. Rev. C* **87**, 014315 (2013).

[47] J. Barea, J. Kotila, and F. Iachello, *Phys. Rev. C* **91**, 034304 (2015).

[48] P. K. Rath, R. Chandra, K. Chaturvedi, P. Lohani, P. K. Raina, and J. G. Hirsch, *Phys. Rev. C* **88**, 064322 (2013).

[49] T. R. Rodriguez and G. Martinez-Pinedo, *Phys. Rev. Lett.* **105**, 252503 (2010).

[50] L. S. Song, J. M. Yao, P. Ring, and J. Meng, *Phys. Rev. C* **90**, 054309 (2014).

[51] A. Faessler, V. Rodin, and F. Simkovic, *J. Phys. G* **39**, 124006 (2012).

[52] P. Vogel, *J. Phys. G* **39**, 124002 (2012).

[53] F. Simkovic, V. Rodin, A. Faessler, and P. Vogel, *Phys. Rev. C* **87**, 045501 (2013).

[54] J. Hyvarinen and J. Suhonen, *Phys. Rev. C* **91**, 024613 (2015).

[55] J. D. Holt and J. Engel, *Phys. Rev. C* **87**, 064315 (2013).

[56] R. A. Sen'kov and M. Horoi, *Phys. Rev. C* **93**, 044334 (2016).

[57] B. A. Brown, D. L. Fang, and M. Horoi, *Phys. Rev. C* **92**, 041301 (2015).

[58] M. Doi, T. Kotani, and E. Takasugi, *Prog. Theor. Phys. Suppl.* **83**, 1 (1985).

[59] S. Stoica and M. Mirea, *Phys. Rev. C* **88**, 037303 (2013).

[60] R. Arnold, C. Augier, A. M. Bakalyarov, J. D. Baker, A. S. Barabash, A. Basharina-Freshville, S. Blondel, S. Blot, M. Bongrand, V. Brudanin, et al. (NEMO-3 Collaboration), *Phys. Rev. D* **93**, 112008 (2016).

[61] M. Agostini, M. Allardt, A. Bakalyarov, M. Balata, I. Barabanov, L. Baudis, C. Bauer, E. Bellotti, S. Belogurov, S. Belyaev, et al. (GERDA Collaboration), *Nature* **544**, 47 (2017).

[62] *Latest results from NEMO-3 and status of the SuperNEMO Experiment* (2016), http://neutrino2016.iopconfs.org/IOP/media/uploaded/EV10P/event_948/10.25__5__waters.pdf.

[63] K. Alfonso, D. R. Artusa, F. T. Avignone, O. Azzolini, M. Balata, T. I. Banks, G. Bari, J. W. Beeman, F. Bellini, A. Bersani, et al. (CUORE Collaboration), *Phys. Rev. Lett.* **115**, 102502 (2015), URL <http://link.aps.org/doi/10.1103/PhysRevLett.115.102502>.

[64] A. Gando, Y. Gando, T. Hachiya, A. Hayashi, S. Hayashida, H. Ikeda, K. Inoue, K. Ishidoshiro, Y. Karino, M. Koga, et al. (KamLAND-Zen Collaboration), *Phys. Rev. Lett.* **117**, 082503 (2016), URL <https://link.aps.org/doi/10.1103/PhysRevLett.117.082503>.

[65] M. Doi, T. Kotani, H. Nishiura, and E. Takasugi, *Progr. Theor. Exp. Phys.* **69**, 602 (1983).

[66] W. Rodejohann, *J. Phys. G* **39**, 124008 (2012).

[67] R. N. Mohapatra and J. C. Pati, *Phys. Rev. D* **11**, 566 (1975).

- [68] M. Hirsch, H. KlapdorKleingrothaus, and S. Kovalenko, Phys. Rev. D **53**, 1329 (1996).
- [69] S. Kolb, M. Hirsch, and H. V. Klapdor-Kleingrothaus, Phys. Rev. D **56**, 4161 (1997).
- [70] A. Faessler, T. Gutsche, S. Kovalenko, and F. Šimkovic, Phys. Rev. D **77**, 113012 (2008).
- [71] J. Suhonen and O. Civitarese, Phys. Rep. **300**, 123 (1998).
- [72] J. Kotila and F. Iachello, Phys. Rev. C **85**, 034316 (2012).
- [73] M. Horoi and A. Neacsu, Adv. High Energy Phys. **2016**, 7486712 (2016).
- [74] J. D. Vergados, H. Ejiri, and F. Simkovic, Rep. Prog. Phys. **75**, 106301 (2012).
- [75] D. Stefanik, R. Dvornicky, F. Simkovic, and P. Vogel, Phys. Rev. C **92**, 055502 (2015), arXiv:1506.07145 [hep-ph].
- [76] K. Muto, E. Bender, and H. Klapdor, Z. Phys. A - Atomic Nuclei **334**, 187 (1989).
- [77] A. Faessler and F. Simkovic, Journal of Physics G: Nuclear and Particle Physics **24**, 2139 (1998), URL <http://stacks.iop.org/0954-3899/24/i=12/a=001>.
- [78] A. Wodecki, W. A. Kamiński, and F. Šimkovic, Phys. Rev. D **60**, 115007 (1999).
- [79] G. Prezeau, M. Ramsey-Musolf, and P. Vogel, Phys. Rev. D **68**, 034016 (2003).
- [80] T. Peng, M. J. Ramsey-Musolf, and P. Winslow, Phys. Rev. D **93**, 093002 (2016).
- [81] F. F. Deppisch, J. Harz, W.-C. Huang, M. Hirsch, and H. Päs, Phys. Rev. D **92**, 036005 (2015).
- [82] F. Ahmed, A. Neacsu, and M. Horoi, Physics Letters B **769**, 299 (2017).
- [83] Z. Maki, M. Nakagawa, and S. Sakata, Prog. Theor. Phys. **28**, 870 (1962), URL <http://dx.doi.org/10.1143/PTP.28.870>.
- [84] J. Beringer, J. F. Arguin, R. M. Barnett, K. Copic, O. Dahl, D. E. Groom, C. J. Lin, J. Lys, H. Murayama, C. G. Wohl, et al. (Particle Data Group), Phys. Rev. D **86**, 010001 (2012).
- [85] S. L. Adler, E. W. Colglazier, J. B. Healy, I. Karliner, J. Lieberman, Y. J. Ng, and H. S. Tsao, Phys. Rev. D **11**, 3309 (1975), URL <http://link.aps.org/doi/10.1103/PhysRevD.11.3309>.
- [86] A. Faessler, S. Kovalenko, and F. Šimkovic, Phys. Rev. D **58**, 115004 (1998).
- [87] F. Simkovic, A. Faessler, H. Muether, V. Rodin, and M. Stauf, Phys. Rev. C **79**, 055501 (2009).
- [88] M. Honma, T. Otsuka, B. A. Brown, and T. Mizusaki, Eur. Phys. J. A **25 Suppl. 1**, 499 (2005).
- [89] M. Honma, T. Otsuka, T. Mizusaki, and M. Hjorth-Jensen, Phys. Rev. C **80**, 064323 (2009).
- [90] C. Qi and Z. X. Xu, Phys. Rev. C **86**, 044323 (2012).